Circuit Modeling on Polyaniline Functionalized Nanowire-Templated Micro-Interdigital Capacitors for pH Sensing

Vlad Andrei Antohe, Adrian Radu, Stefan Mátéfi-Tempfli, and Luc Piraux

***Abstract*—This study presents an improved alternative current (*ac*) circuit modeling of a highly sensitive capacitive *pH*-sensing element based on polyaniline (*PANI*) functionalized nanowire-templated micro-interdigited electrodes (*NWs μIDEs*). While electrical resonance measurements deal with a total equivalent capacity, comparative investigations show a good agreement with the fitting parameters of the corresponding model. A physical interpretation of the model is discussed to help in understanding the detection mechanism and a possible methodology to be used for further integration of the subsequent device is suggested.**

***Index Terms*—Alumina templates, equivalent circuit modeling, *pH* sensors, *Pt* interdigital capacitors, *Pt* nanowires.**

I. Introduction

In THE past decade, localized nanowires functionalized with different types of organic layers have received considerable attention for potential application in nano-/micro- sized capacitive sensing devices owing to their inherent properties of small size, high mechanical strength and not in the least, large active surfaces that generate higher sensitivities [1]–[3]. Microelectrodes directly patterned on Si/SiO_2 substrates represent a frequent choice in the fabrication of biochemical sensors due to their production simplicity and compatibility with standard *Si* low-cost processing on large areas [4], [5]. Sensitive pH detection has been extensively searched lately, due to its potential application in biological processes or acidic life-environment real-time monitoring [6]–[10].

In a previous paper [10], we have shown a highly sensitive pH sensor based on *PANI* functionalized *NWs μIDEs*. By increasing its active surface using vertically aligned nanowires, high detection sensitivities have been obtained.

Manuscript received May 17, 2010; revised January 12, 2011; accepted March 23, 2011. Date of publication April 7, 2011; date of current version November 9, 2011. This work was supported by the Government of the Walloon Region from Belgium (*NANOTIC – FEELING* Research Program). The review of this paper was arranged by Associate Editor Sorin D. Cotofana.

V. A. Antohe, S. Mátéfi-Tempfli, and L. Piraux are with the Institute of Condensed Matter and Nanosciences (ICMN), Université Catholique de Louvain, 1348 Louvain-la-Neuve, Belgium (e-mail: vlad.antohe@uclouvain.be, matefi@uclouvain.be, luc.piraux@uclouvain.be).

A. Radu is with the Department of Materials and Electronic & Optoelectronic Devices, University of Bucharest, 077125 Bucharest, Romania (e-mail: adrian.radu@fizica.unibuc.ro).

Color versions of one or more of the figures in this paper are available online at http://ieeexplore.ieee.org.

Digital Object Identifier 10.1109/TNANO.2011.2136384

The capacitive measurements were based on monitoring the frequency response of a parallel *LC* circuit, built by adding an external inductance on top of the brush-structure. Large shifts in the resonance frequency have also been obtain by tuning the thickness of the functional layer, leading to sensitivity improvements of up to two orders of magnitude higher, compared with conventional pH sensors. The entire setup was based on measuring a relative capacity change between different pH values. Unfortunately, the detection mechanism is not well understood, on base of a general equivalent electrical circuit that has been extensively used until now. As a consequence, further investigations of *ac* modeling are always required in such situations [13]. Here, we propose an improved capacitive detection algorithm, based on a transitory regime signal analysis. The results obtained are in good agreement with the resonance measurements, leading to a better interpretation of the corresponding *ac* electrical model.

II. Fabrication and Measurements of NWs μIDEs

A. PANI NWs μIDEs and Resonance Measurements

As previously described [9]–[12], the entire fabrication process was a blending between lithographic techniques and electrochemical synthesis within supported nanoporous alumina (Al_2O_3) templates (see Fig. 1). *Pt μIDEs* were first patterned on a Si/SiO_2 substrate, being further masked by an SiN_x layer that has protected the contacts against the subsequent electrochemical synthesis [Fig. 1(a)]. The nanoporous alumina ($\sim$1.5 μm) was built on top of the interdigited metallic pads by anodization of a thick aluminum layer ($\sim$1 μm) previously sputtered on the entire surface using a *Plassys MP*500 magnetron sputtering equipment. The oxidation of *Al* in 0.3 M oxalic acid, at 2 °C, with an anodic voltage of 60 V (applied from a *Keithley* 2400 source) coupled with an enlargement process of the pores in 0.5 M orthophosphoric acid, at $\sim$30 °C, has led to nanopores formation of $\sim$90 nm in diameter and $\sim$150 nm interspaced [14]. *Pt* was further electrodeposited inside the nanopores using a commercial *Pt* electrolyte (*Metakem*) at $\sim$50 °C, by applying $-$ 0.3 V (versus an Ag/AgCl reference electrode) from a *PAR 263 A Potentiostat*. Finally, the alumina and remaining aluminum have been removed in a *2* M NaOH solution for 10 min. at room temperature and then the sample was thoroughly rinsed. Thin layers of polyaniline were polymerized using an electroless process (with *Pt* acting as catalyst) in an oxygen-saturated solution of aniline (0.4 M) and H_2SO_4 (0.4 M) at 15 °C for immersion timings of up to 3 h. [Fig. 1(b)]. In a very last step, the *PANI* has

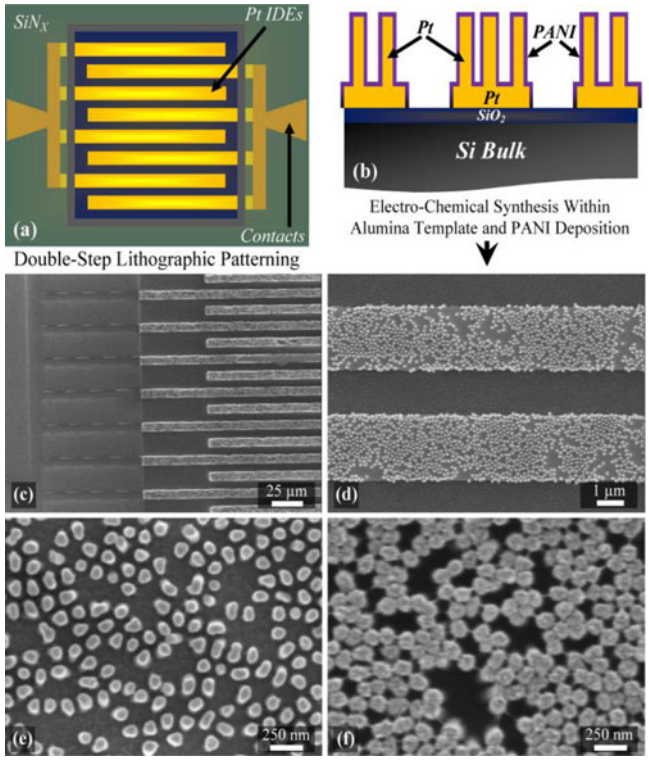

Fig. 1. (a) Schematic draw of the SiN_x masked *Pt* micro-interdigited electrodes (*μIDEs*), defined by a double step photolithographic patterning. (b) Schematic view of vertically-aligned nanowires (*NWs*) grown on top of *μIDEs* by an electrochemical synthesis within the nanopores of the Al_2O_3 template. (c-e) Scanning electron microscope (*SEM*) micrographs of *Pt NWs* synthesized on top of *Pt μIDEs*, with increased magnification from (c) to (e). The protection role of the *SiNx* masking layer can be noticed in panel (c). (f) Increased magnification *SEM* image of *Pt NWs μIDEs*, covered by a thin layer (∼30 nm) of polyaniline (*PANI*). The thin polymer layer protrudes between the nanowires, taking their shapes and maintaining the high active surface of the nanostructured sample [9], [10].

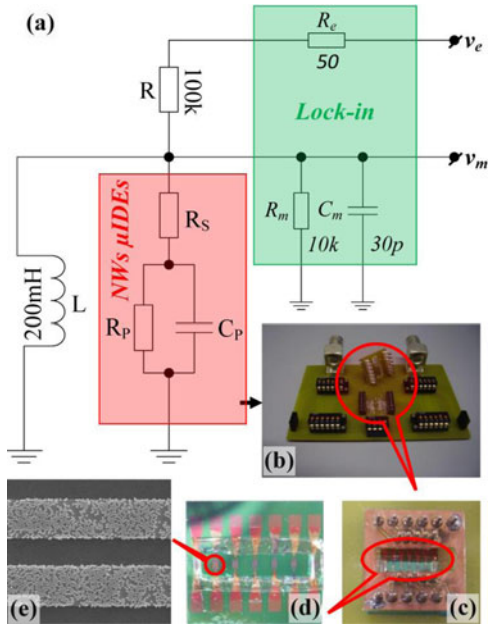

Fig. 2. (a) The electronic circuit used for resonance measurements on the *PANI Pt NWs μIDEs* samples. An *LC* resonator was built by adding an external inductance (*L*) of ∼200 mH. (b) The printed circuit board (*PCB*) used for contacting, manipulating, and switching between *μIDEs* structures. (c) Magnification of contacting area, using a spring-probes based cage. (d) A silicone well confining the active area of up to five structures, for dropping *pH*-test solutions. (e) *SEM* magnified active area of the sensor being measured in different *pH* environments.

been undoped with 1 M NH_4OH solution for 30 min. [15]–[17]. Scanning electron microscope (SEM) images of the *Pt NWs μIDEs* are shown in Fig. 1(c, d, e) with increased magnification from (c) to (e) and a *PANI* sensitized zoomed area in panel (f).

Various electrochemical impedance spectroscopy (EIS) investigations [18]–[20], as well as previous reports [9], [10] claimed that the above mentioned samples can be acceptably modeled with a simple parallel *RC* group (R_PC_P in Fig. 2) with a small series resistive component (R_S) of the pH solution included. In this way, resonance measurements have been performed on the configuration depicted in Fig. 2(a), using a *7265 DSP Lock-in Amplifier* for frequency sweeping. The entire electronic setup [especially designed printed circuit boards — *PCBs*, for contacting and manipulating the samples—Fig. 2(b), as well as silicone wells for dropping off ∼10 μl of different pH buffers of constant conductivity around 11 mS/cm — Fig. 2(d)] facilitated the capacitive measurements. They were based on a relative change of a total capacity (C_T) estimated with (1a), where f_r is the resonance frequency of the corresponding *LC* resonator and *L* is the added external inductance of 0.2 H.

The setup in Fig. 2(a) allowed also to estimate an overall resistive component (R_T) using (1b), where V_e, V_m are the excitation (lock-in provided) and measured voltage, respectively, in the circuit, *R* is an external limiting current resistance and R_m is the input internal resistive part of the lock-in device. For the calculations below R_S was neglected, as well as R_e (lock-in output resistance) and C_m (the input internal capacity of the lock-in). Regarding (1b), based on the aforementioned conditions, R_T should result in the same range as *PANI* intrinsic resistance (R_P). Comparative frequency response measurements on low active surface (*LAS - NWs*-free *μIDEs*) and high active surface (*HAS - NWs*-templated *μIDEs*) detectors, respectively, are shown in Fig. 3(a, b) for different acidic environments (pH 2 to pH 7).

$$\begin{cases} f_r = \dfrac{1}{2\pi\sqrt{LC_T}} \Rightarrow C_T = \dfrac{1}{4\pi^2 f_r^2 L} & \text{(1a)} \\ R_T \cong R_P = V_m \dfrac{RR_m}{V_e R_m - V_m(R + R_m)} & \text{(1b).} \end{cases} \quad (1)$$

Both architectures were functionalized with ∼30 nm *PANI*. The resonance frequency shifts were larger in the favor of the *HAS* situation - see Fig. 3(b) [9]. Fig. 3(c) shows a full-range sensitivity comparison that underlines the advantages of using vertically-aligned nanowires decorated microelectrodes. By nanostructuring their active surface, the sensitivity has been increased with up to two orders of magnitude in respect to the *LAS* sensor.

The data shown in Fig. 3(c, d) and Table I reveal the fact that not only the overall capacity has been increased, but also the relative changing between pHs [10]. Unfortunately, as previously

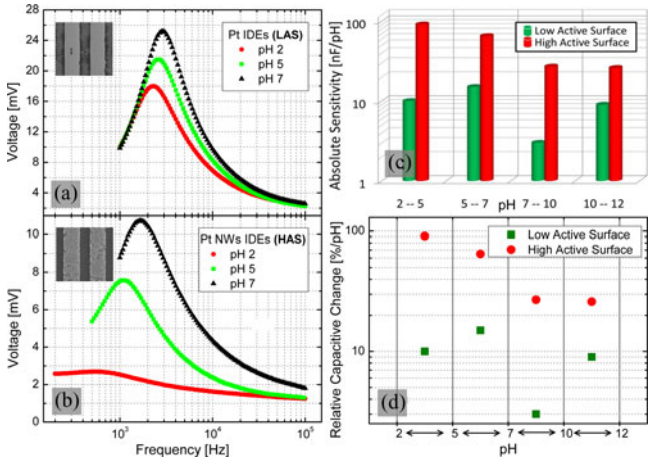

Fig. 3. (a, b) Comparative frequency responses between low active surface (*LAS*) – above and high active surface (*HAS*) – below, measured in 3 acidic environments (*pH* 2 – red circles, *pH* 5 – green squares and *pH* 7 – black triangles). (c) Absolute sensitivity comparison between *LAS* (green) and *HAS* (red) sensors, respectively, on the entire *pH* range. (c) Relative capacitive change between different *pHs* corresponding to *LAS* (green squares) and *HAS* (red circles) structures, respectively [10].

TABLE I
SUMMARY OF THE ABSOLUTE/RELATIVE SENSITIVITY EXPERIMENTAL DATA (*LAS* – LOW ACTIVE SURFACE SENSOR, *HAS* – HIGH ACTIVE SURFACE SENSOR). THE THICKNESS OF THE *PANI* FUNCTIONAL LAYER IS ∼30 nm

Analyzing Environment	Absolute Sensitivity (*nF/pH*)		Relative Change (*%/pH*)	
	LAS	***HAS***	***LAS***	***HAS***
pH 2 ↔ pH 5	1.94	97.18	10	91
pH 5 ↔ pH 7	2.26	30.31	15	65
pH 7 ↔ pH 10	0.46	12.58	3	27
pH 10 ↔ pH 12	1.56	22.49	9	26

mentioned, the model depicted in Fig. 2(a) was an approximation and was mainly focused on the resonance setup. As a result, the *ac* electrical circuit had limited success in interpreting the microscopic sensing mechanism as the resonant frequency change.

B. Transitory Regime Analysis

To better understand the electrical properties related to the underlying mechanism of the resonance frequency shifts upon pH changes, a more consistent and accurate *ac* circuit model is mandatory. Additional information could be obtained by analyzing the sample in transitory regime. A fast multipulse sequence may pass through the device being extracted at the exit port. Starting with the same assumption of the equivalent circuit ($R_S - R_P C_P$), a similar measuring setup is depicted in Fig. 4(a). Fig. 4(b, c) shows simulation diagrams of the voltage/current signals, respectively, through the entire circuit. A multipulse generator applies a square wave sequence (black curve), corresponding to v_i. Blue curve is the voltage (v_{CIDE}) across the internal capacitive component of the sample (C_P) as it may be seen in Fig. 4(a), its real monitoring being of course limited. The output signal v_o [red curve in Fig. 4(b)] was considered after an external resistance R [see Fig. 4(a)]. The corresponding current flowing through the circuit (i_R) can be seen in Fig. 4(c).

The simulation diagrams depicted in Fig. 4(b, c) give access to the computations of model parameters (R_S, R_P, C_P), using step-by-step time analysis. By extracting the pairs (V_1, I_1), (V_2, I_2), and time constant (τ) of the resulted (RC) group, the three above mentioned parameters can be easily computed, using the system (2).

$$\begin{cases} V_1 = V_i \dfrac{R_S}{R + R_S} \;;\; V_2 = V_i \dfrac{R_S + R_P}{R + R_S + R_P} \\ I_1 = V_i \dfrac{1}{R + R_S} \;;\; I_2 = V_i \dfrac{1}{R + R_S + R_P} \\ \tau = C_P \dfrac{R_P (R + R_S)}{R + R_S + R_P}. \end{cases} \tag{2}$$

Following the aforementioned procedure, a square wave signal with a periodicity of 10 ms was generated with a *PAR 263 A Potentiostat* and applied to the circuit. The current flowing through the circuit (i_R) was automatically extracted (with the same device) and computed with a specially designed software algorithm [see Fig. 5(a)]. A closer look (see the emphasized area) reveals that in quite short time (∼500 μs) i_R vanishes to zero, making impossible the calculations using (2) for fitting the parameters of the model depicted in Fig. 4(a). This phenomenon may only be explained if a series capacitive component is present in the *ac* model. That fits quite well with the observations because after the transient period, the "series" capacitor being charged practically blocks any *dc* current (i_R) flowing.

The improved equivalent electrical model is displayed in the inset of Fig. 5(a). This explanation becomes obvious if once the corresponding circuit is interpreted as in Fig. 5(b). By covering the entire surface with a uniform and consistent layer of *PANI*, its intrinsic components (R_P, C_P) are changing as a function of *pH*. Moreover, they can be increased by modifying the thickness of the *PANI* layer itself, as previously reported [10]. Going further and immersing the sample in a well conductive *pH* buffer environment, double layer capacitive components [21], [22] are being formed at the *PANI*/electrolyte interface, components that are strongly affected by the proton concentration of the *pH* buffer values [23], [24]. The active changes in these components give higher sensitivities in acidic environments compared with alkaline ones, as can be noticed in Fig. 3(c, d) [10]. Similar results were also reported elsewhere [25]–[27]. The *pH* buffers are well conductive, resulting in a small resistive component (R_S) that remains unchanged as a function of *pH*, as the different buffers conductivity has been previously adjusted to the same value (∼11 mS/cm) by using *KCl*.

Rigorously, parasite components of the Si/SiO_2 substrate (C_W, R_W) are also present, but are small enough (in respect with the above active components – R_S, C_S, R_P, C_P), so that they could be neglected, as was previously reported [9].

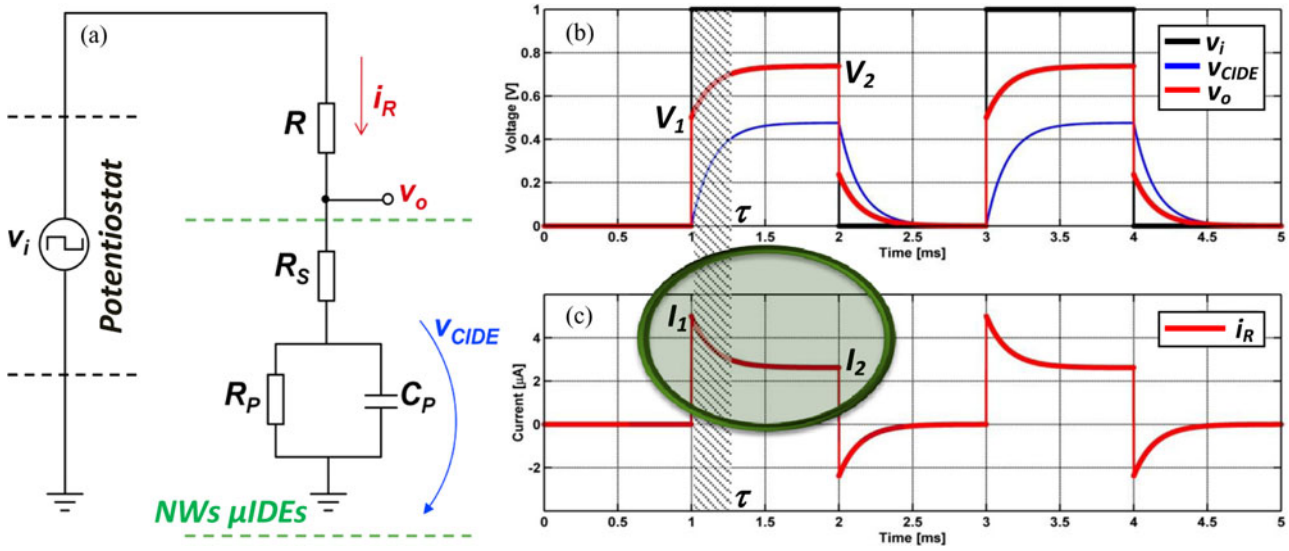

Fig. 4. (a) The electronic circuit used for transitory analysis using a multipulse signal. The pulses were being generated and measured with a *PAR 263 A Potentiostat/Galvanostat*. (b) Simulated voltage signal diagrams on the corresponding circuit (black – the square wave signal that is applied to the sample – v_i, blue – the sample's internal voltage drop – v_{CIDE}, and red – the measured signal – v_o. (c) The corresponding current – i_R flowing through the entire electrical circuit (the emphasized area represents a current semiperiod that is extracted and processed with the potentiostat).

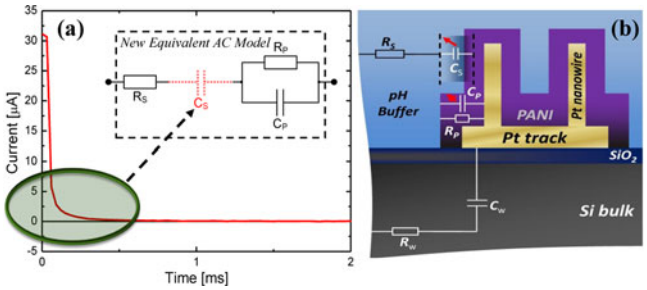

Fig. 5. (a) The first 2 ms from the semiperiod (∼ 5 ms) of the passing current (i_R) through an *NWs μIDEs* sample, covered by ∼30 nm of *PANI*. I_R vanishes in ∼500 μs (see the emphasized area). The inset corresponds to the improved electrical *ac* equivalent circuit, built on base of the transient analysis. (b) Transversal schematic sketch through a *PANI NWS μIDEs* device, showing an interpretation of the equivalent model. C_P and R_P are the intrinsic components of the *PANI* layer, C_S is a double–layer capacity formed at the *PANI* / solution interface, R_S is the *pH* buffer solution resistive component (the buffer shows complex impedance but with a negligible small signal imaginary part for $<10^4$ Hz), and (C_W , R_W) are the parasite components through the substrate.

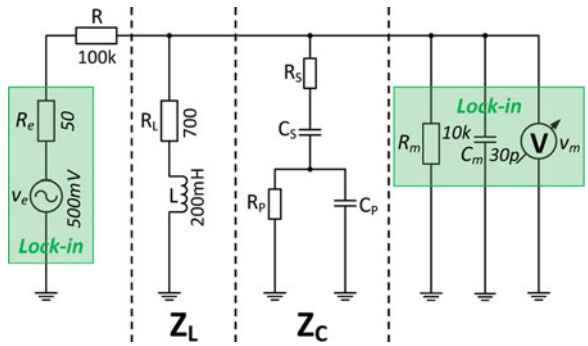

Fig. 6. The complete electronic model used for the complex fitting function that refines the parameters involved in the electrical resonance of the circuit. The internal components of the Lock-in have been considered ($R_e = 50\ \Omega$ and $R_m = 10\ \mathrm{k}\Omega$) as well as the loss resistance of the inductance ($R_L \cong 700\ \Omega$).

C. Further Discussions

As described already in Section *A*, the resonance measurements allowed an easy access in estimating the overall electrical components (C_T, R_T) of the sensor. It would be interesting to reveal their internal changing mechanism. Based on the improved electrical equivalent circuit [inset of Fig. 5(a)], a complex function can be constructed for fitting the resonance experimental data, facilitating the access to R_S, C_S, R_P, and C_P, respectively.

Therefore, a complex fitting function was built on the base of the complete electronic model, depicted in Fig. 6. The internal lock-in resistive input/output components (R_e, R_m) as well as the parasite resistive component of the inductance L ($R_L \cong 700\ \Omega$) have been taken into account. Moreover, the amplitude of the excitation voltage (V_e) was fixed to 0,5 V to recreate the conditions used for the resonance measurements.

The fitting algorithm followed (3), where v_m is the lock-in measured voltage at the exit port, v_e is the input signal and Z is the total impedance of the system.

$$\begin{cases} v_m = v_e \dfrac{Z}{Z + R_e + R} = \mathrm{Re}\{v_m\} + i \cdot \mathrm{Im}\{v_m\} \\ Z = \dfrac{Z_L Z_C R_m}{Z_L Z_C + Z_L R_m + Z_C R_m}. \end{cases} \tag{3}$$

Z_L and Z_C are the local impedances of the inductance and of the total capacitive equivalent model (see Fig. 6), respectively, and are given by (4), where $X_L = i \cdot \omega L$ is the inductive reactance of L and $X_S = -i/\omega C_S$, $X_P = -i/\omega C_P$ are the capacitive reactance of C_S and C_P, respectively ($\omega = 2\pi f$).

$$\begin{cases} Z_L = R_L + X_L \\ Z_C = R_S + X_S + \dfrac{R_P X_P}{R_P + X_P}. \end{cases} \tag{4}$$

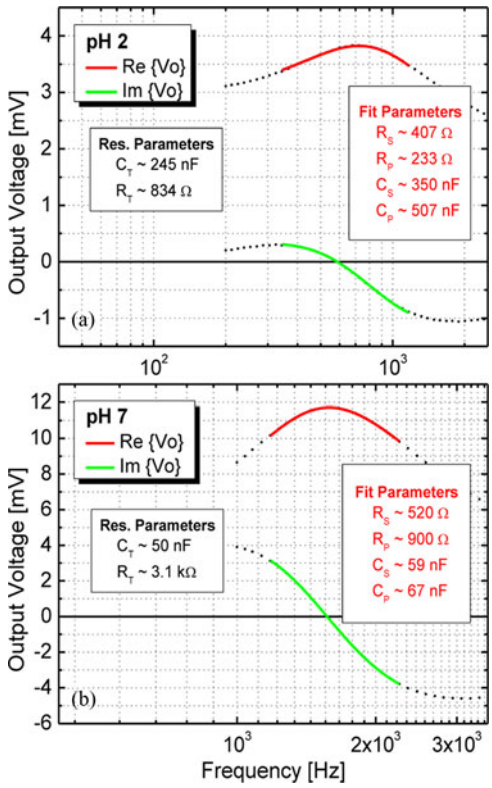

Fig. 7. Electrical resonance plots for real (upper curves) and imaginary (lower curves) parts of the output signal (v_m), measured for *pH 2* (a) and *pH 7* (b) on a *PANI Pt NWS μIDEs* device (~30 nm *PANI*). Fitting results of both real (in red) and imaginary (in green) parts of v_m are shown. A good agreement between the resonance measurement results and the fitting computations can be noticed.

For higher accuracy, the entire measured signal (v_m) has been split in its real and imaginary complex components ($Re\{v_m\}$ and $Im\{v_m\}$, respectively [see (3)], so that the fitting algorithm performs a dual computation of the corresponding coefficients (the model parameters: R_S, C_S, R_P, C_P).

Fig. 7(a, b) recalls two resonance plots, corresponding to pH 2 – Fig. 7(a) and pH 7 – Fig. 7(b), respectively. The upper curves are related with real part of the output signals, while the lower ones are linked with their imaginary part. Both measurements are performed on the same *Pt NWs μIDEs* structure sensitized by ~30 nm of *PANI*. The red and green curves correspond to the fitting results of the real and imaginary parts. The fitting range was limited around the resonance peak for avoiding other low and/or high frequency-related phenomena to be considered. The plots in Fig. 7 reveal a very good agreement between theoretical and experimental results, being a confirmation of the correctness of the improved equivalent *ac* circuit [inset of Fig. 5(a)]. Due to a strong hysteresis of the *PANI pH* response toward alkaline *pHs* demonstrated elsewhere [25], only acidic range has been validated. On the other hand, in biomedical applications, the acidic range monitoring is highly required. Fig. 8(a, b) shows the entire acidic pH range dependence of each model parameter, including the resonance results (see also Table II).

Concerning the capacitive behavior, the total capacity C_T extracted from the simple *LC* resonance, rigorously follows the exponential dependence [21], [26] of the model components

TABLE II
COMPARISON BETWEEN EXPERIMENTAL AND THEORETICAL RESULTS CONCERNING THE EXTRACTION OF THE *AC* MODEL COEFFICIENTS FOR THE ACIDIC pH RANGE

pH Solution	Fitting Coefficients				Resonance Results	
	R_S (Ω)	R_P (Ω)	C_S (*nF*)	C_P (*nF*)	R_T (Ω)	C_T (*nF*)
2	407	233	350	507	834	245
5	386	603	105	124	2100	97
7	520	900	59	67	3100	50

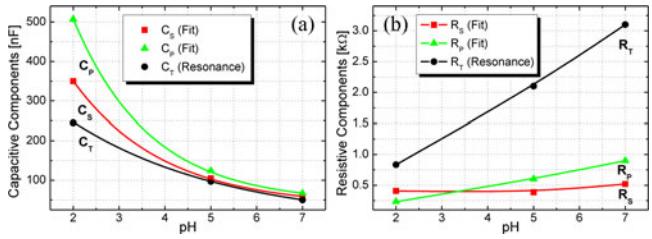

Fig. 8. Independent capacitive (a) and resistive (b) components versus *pH*. The good agreement between capacitive model components and their corresponding resonance results can be noticed, together with their exponential behavior (a). R_S can be easily linked with a small and constant *pH* buffer resistive component, while R_P is changing as a function of *pH* (b). The higher *pH* sensitivity and stability achieved by the capacitive detection approach can be noticed as well.

(intrinsic polyaniline part C_P and double layer component C_S) as can be noticed in Fig. 8(a). As regarding the resistive dependence [Fig. 8(b)], the relatively small R_S is almost constant on the entire range, proving the assumption of representing the resistive part of the pH solution (in which *dc*-conductivity was rigorously tuned of being the same among the different pH buffers [9], [10]). Nevertheless, it shows a small drift toward neutral values. This behavior could be explained by a small frequency dependence of R_S, as the resonance frequency peak depends on the pH. Regarding the intrinsic *PANI* resistive component (R_P), the pH dependence shows smaller values toward pH 2 because of the changes in its oxidation states [10], [21]. However, the relatively high value and the high variation of the total resistive component R_T estimated roughly by (1b) from the resonance measurement is not properly explainable. All of these, point out that the simplistic equation (1b) is not really holding while the complex fitting with the system (3) gives the correct intrinsic R_P, R_S and also C_P, C_S values.

III. CONCLUSION

As a general conclusion polyaniline sensitized vertically-aligned nanowire-decorated micro-electrodes have been developed on top of Si/SiO_2 bulk wafers, by combining lithographic techniques with electro-chemical synthesis within alumina templates. The complete brush structure serves as a pH-sensing element with higher detection efficiency. The nanostructured design acts as an interdigital capacitor with very high surface, leading to large overall electrical capacity increases. By introducing the device in an *LC* resonator, large shifts in its resonant frequency have been noticed while applying different

pHs. Going further, a transient regime analysis on the device has been performed using a 100 Hz square-wave sequence. The results have proved the existence of a double-layer capacity, which generally is well-known to be formed at any electrode-electrolyte interface. As a consequence, an improved *ac* equivalent circuit model for the capacitive nanowire-templated pH sensor was presented. In addition, the intrinsic sensing mechanism has been investigated in terms of the self - resonant frequency of the sample introduced in the *LC* resonator. The subsequent *ac* model was further confirmed by the complex fitting calculations that have led access to each model parameters. The capacitive components were in excellent agreement with the resonance results meaning that the capacitive detection is the most advantageous approach, for further integration within Si processing. The proposed pH sensor has several advantages: 1) it employs a simple and efficient detection mechanism, 2) it is low-cost, and 3) it allows an easy functionalization. Moreover, its unique brush-architecture, leads to higher sensitivities compared with conventional sensors. It is worth pointing out that the novel frequency based pH sensor has potential in wireless remote sensing applications, for real time *in situ* monitoring. The described architecture may be also used for detection of specific biomolecular bindings (like antigen–antibody reactions or *DNA* hybridization), by adequately choosing the functional layer.

ACKNOWLEDGMENT

The authors thank Augustin Duţu and Sorin Melinte for providing the *μIDEs* patterned Si/SiO_2 substrates. They also thank Sami Yunus, Anne Attout, and Patrick Bertrand for *PCBs* design and *PANI* synthesis.

REFERENCES

[1] U. Yogeswaran and S.-M. Chen, "A review on the electrochemical sensors and biosensors composed of nanowires as sensing material," *Sensors*, vol. 8, no. 1, pp. 290–313, Jan. 2008.

[2] J. Wang, "Biomolecule-functionalized nanowires: From nanosensors to nanocarriers," *Chem.Phys.Chem.*, vol. 10, no. 11, pp. 1748–1755, Jul. 2009.

[3] Y. Lu, M. Yang, F. Qu, G. Shen, and R. Yu, "Enzyme-functionalized gold nanowires for the fabrication of biosensors," *Bioelectrochemistry*, vol. 71, no. 2, pp. 211–216, Nov. 2007.

[4] P. Van Gerwen, W. Laureyn, W. Laureys, G. Huyberechts, M. O. De Beeck, K. Baert, J. Suls, W. Sansen, P. Jacobs, L. Hermans, and R. Mertens, "Nanoscaled interdigitated electrode arrays for biochemical sensors," *Sensors Actuators B: Chem.*, vol. 49, no. 1/2, pp. 73–80, Jun. 1998.

[5] K. Toda, Y. Komatsu, S. Oguni, S. Hashiguchi, and I. Sanemasa, "A planar gas sensor combined with interdigitated array electrodes," *Anal. Sci.*, vol. 15, no. 1, pp. 87–89, Jan. 1999.

[6] X. Zeng-Hong, G. Liang-Qia, Z. Xiang-Hua, Z. Mao-Sheng, and C. Guo-Nan, "Research of pH-sensitive functional material," *Analytical Sciences*, vol. 17, no. Suppl., pp. a151–a153, 2001.

[7] M. Yuqing, C. Jianrong, and F. Keming, "New technology for the detection of pH," *J. Biochem. Biophys. Methods*, vol. 63, pp. 1–9, Feb. 2005.

[8] S. Bhattarai, K. H. Aschenbach, and R. D. Gomez, "Carbon nanotube based aqueous ion and pH sensor," *Maryland Eng. Res. Internship Teams: Biosyst. Internships Engineers (Merit Bien),* Technical Report, pp. 1–5, 2009.

[9] V. A. Antohe, A. Radu, S. Yunus, A. Attout, P. Bertrand, M. Mátéfi-Tempfli, L. Piraux, and S. Mátéfi-Tempfli, "A versatile method to grow localized arrays of nanowires for highly sensitive capacitive devices," *J. Optoelectron. Adv. Mat.*, vol. 10, no. 11, pp. 2936–2941, Nov. 2008.

[10] V. A. Antohe, A. Radu, M. Mátéfi-Tempfli, A. Attout, S. Yunus, P. Bertrand, C. A. Duţu, A. Vlad, S. Melinte, S. Mátéfi-Tempfli, and L. Piraux, "Nanowire-templated microelectrodes for high-sensitivity pH detection," *Appl. Phys. Lett.*, vol. 94, p. 073118, 2009.

[11] S. Mátéfi-Tempfli, M. Mátéfi-Tempfli, A. Vlad, V. A. Antohe, and L. Piraux, "Nanowires and nanostructures fabrication using template methods: A step forward to real devices combining electrochemical synthesis with lithographic techniques," *J. Mater. Sci.: Mater. Electron.*, vol. 20, pp. 249–254, 2009.

[12] A. Vlad, M. Mátéfi-Tempfli, V. A. Antohe, S. Faniel, N. Reckinger, B. Olbrechts, A. Crahay, V. Bayot, L. Piraux, S. Melinte, and S. Mátéfi-Tempfli, "Nanowire-Decorated Microscale Metallic Electrodes," *Small*, vol. 4, no. 5, pp. 557–560, 2008.

[13] H.-J. Lee, H.-S. Lee, H. H. Choi, K.-H. Yoo, and J.-G. Yook, "An RF circuit model for interdigital capacitors-based carbon nanotube biosensors," *IEEE Trans. Nanotechnol.*, vol. 9, no. 6, pp. 682–686, Nov. 2010.

[14] S. Mátéfi-Tempfli, "Nanostructures grown via electrochemical template methods: Synthesis, measurements and applications," in *Encyclopedia of Nanotechnology*, E. D. Carlson, Ed. New York: Nova Science Publishers, 2009, pp. 459–481.

[15] A. Attout, S. Yunus, and P. Bertrand, "Electroless deposition of polyaniline: Synthesis and characterization," *Surf. Interface Anal.*, vol. 40, pp. 657–660, Jan. 2008.

[16] S. Yunus, A. Attout, and P. Bertrand, "Controlled aniline polymerization strategies for polyaniline micro- and nano self-assembling into practical electronic devices," *Langmuir*, vol. 25, no. 3, pp. 1851–1854, Jan. 2009.

[17] C. Liao and M. Gu, "Electroless deposition of polyaniline film via autocatalytic polymerization of aniline," *Thin Solid Films*, vol. 408, pp. 37–42, Jan. 2002.

[18] H. Li, J. Wang, Q. Chu, Z. Wang, F. Zhang, and S. Wang, "Theoretical and experimental specific capacitance of polyaniline in sulfuric acid," *J. Power Sources*, vol. 190, no. 2, pp. 578–586, Jan. 2009.

[19] M. Kalaji and L. M. Peter, "Optical and electrical A. C. response of polyaniline films," *J. Chem. Soc. Faraday Trans.*, vol. 87, no. 6, pp. 853–860, 1991.

[20] A. S. Sarac, M. Ates, and B. Kilic, "Electrochemical impedance spectroscopic study of polyaniline on platinum, glassy carbon and carbon fiber microelectrodes," *Int. J. Electrochem. Sci.*, vol. 3, pp. 777–786, May 2008.

[21] K. -H. Lubert and L. Dunsch, "The influence of protons on the impedance of polyaniline films," *Electrochim. Acta*, vol. 43, no. 7, pp. 813–822, Dec. 1997.

[22] Y. Lauw, M. D. Horne, T. Rodopoulos, A. Nelson, and F. A. M. Leermakers, "Electrical double-layer capacitance in room temperature ionic liquids: Ion-size and specific adsorption effects," *J. Phys. Chem. B*, vol. 114, no. 34, pp. 11149–11154, Aug. 2010.

[23] A. G. Macdiarmid, J. C. Chiang, A. F. Richter, and A. J. Epstein, "Polyaniline: A new concept in conducting polymers," *Synth. Metals*, vol. 18, pp. 285–290, Feb. 1987.

[24] E. T. Kang, K. G. Neoh, and K. L. Tan, "Polyaniline: A polymer with many interesting intrinsic redox states," *Prog. Polymer Sci.*, vol. 23, no. 2, pp. 277–324, Jul. 1998.

[25] T. Lindfors and A. Ivaska, "pH sensitivity of polyaniline and its substituted derivatives," *J. Electroanal. Chem.*, vol. 531, no. 1, pp. 43–52, Aug. 2002.

[26] K. Hamdani and K. L. Cheng, "Polyaniline pH Electrodes," *Microchem. J.*, vol. 61, no. 3, pp. 198–217, Mar. 1999.

[27] T. Lindfors, S. Ervelä, and A. Ivaska, "Polyaniline as pH-sensitive component in plasticized PVC membranes," *J. Electroanal. Chem.*, vol. 560, no. 1, pp. 69–78, Dec. 2003.

Vlad A. Antohe was born in Bucharest, Romania, on October 11, 1979. He received the B.Sc. degree in physics education, in 2002, and M.Sc. degree in electronics and metrology, in 2005, from the Faculty of Physics, University of Bucharest, Romania. He also obtained M.Eng. degree in electronics and telecommunications from the Faculty of Electronics and Telecommunications, Politechnique University of Bucharest, in 2003. He is currently a Ph.D. student with the Institute of Condensed Matter and Nanosciences (ICMN), Catholic University of Louvain (UCL), Louvain-la-Neuve, Belgium.

His main research interests are in the areas of nanotechnology, nanomaterials for sensors and biosensors, nanostructured sensors based on nanowire arrays, as well as electrical properties and circuit modeling of polymer–functionalized nanowires with sensing features.

Adrian Radu received the B.Sc. degree in physics, in 2006, and M.Sc. degree in electronics and metrology, in 2008, from the Faculty of Physics, University of Bucharest, Romania. He is currently a Ph.D. student with the Department of Materials and Electronic & Optoelectronic Devices (MDEO), University of Bucharest, Romania.

His main research interests are in the areas of nanotechnology, nanomaterials for electronic and optoelectronic devices, nanostructures development for photovoltaic applications, as well as electrical and optical characterization of 4th generation solar cells.

Stefan Mátéfi-Tempfli received the M.Sc. degree, in 1985, at the Institute of Technology Cluj and, in 1996, at the University of Oradea, Romania. He received the Ph.D. degree from the University of Pitesti, in 2001.

He is a Senior Research Associate at the Institute of Condensed Matter and Nanosciences (ICMN), Université Catholique de Louvain (UCL), Louvain-la-Neuve, Belgium, and Visiting Senior Lecturer at the Facultés Universitaires Notre-Dame de la Paix (FUNDP), Namur, Belgium. He possesses more than 115 scientific outputs and holds 3 patents. He has a broad research interest with particular focus on nanomaterials' synthesis, especially by template methods, their chemical and physical properties, such as magnetic and superconducting, and applications in various fields of electronics, sensors and biosensors, bionanotechnology, heterogeneous catalysis, photovoltaics, non-linear optics and metamaterials.

Luc Piraux received the Ph.D. degree, in 1987, from the University of Louvain, Belgium and was Research Associate of the National Fund for Scientific Research, Belgium, in the period of 1989–2001. He is currently a Full Professor with the Institute of Condensed Matter and Nanosciences (ICMN), Université catholique de Louvain (UCL), Louvain-la-Neuve, Belgium.

His research activity at ICMN deals with basic experimental research in the field of nanostructured materials and low-dimensional systems, including the investigation of both their physical properties and their synthesis with the aim of generating new structural arrangements tailored to specific desired properties. Prof. L. Piraux research team has expertise in the fabrication of magnetic and superconducting nanowires as well as magnetic multilayered nanowires grown by electrodeposition in nanoporous materials. The group also has expertise in the fabrication of well-ordered nanoporous materials using alumina templates. His current research activities are in the field of spintronics, nanomagnetism, low-dimensional superconductivity, vortex dynamics, development of microwave devices and of nano-biosensors. He has published more than 200 refereed papers and holds 3 patents. He was involved in several European research projects and has managed many national projects.